Effective Hamiltonian for Photonic Topological Insulator with Non-Hermitian Domain Walls

Yandong Li,[1,*] Chongxiao Fan,[1,2,3,*] Xiaoyong Hu,[1,4,5,†] Yutian Ao,[1] Cuicui Lu,[6,‡] C. T. Chan,[7,§] Dante M. Kennes,[2,3] and Qihuang Gong[1,4,5]

[1]*State Key Laboratory for Mesoscopic Physics & Department of Physics, Collaborative Innovation Center of Quantum Matter and Frontiers Science Center for Nano-optoelectronics, Beijing Academy of Quantum Information Sciences, Peking University, Beijing 100871, People's Republic of China*

[2]*Institute for Theory of Statistical Physics, RWTH Aachen University, and JARA Fundamentals of Future Information Technology, 52062 Aachen, Germany*

[3]*Max Planck Institute for the Structure and Dynamics of Matter, Center for Free Electron Laser Science, Hamburg, Germany*

[4]*Peking University Yangtze Delta Institute of Optoelectronics, Nantong, Jiangsu 226010, People's Republic of China*

[5]*Collaborative Innovation Center of Extreme Optics, Shanxi University, Taiyuan, Shanxi 030006, People's Republic of China*

[6]*Laboratory of Advanced Optoelectronic Quantum Architecture and Measurements of Ministry of Education, Beijing Key Laboratory of Nanophotonics and Ultrane Optoelectronic Systems, School of Physics, Beijing Institute of Technology, Beijing 100081, People's Republic of China*

[7]*Department of Physics, The Hong Kong University of Science and Technology, Clear Water Bay, Kowloon, Hong Kong, China*

(Received 2 March 2022; accepted 12 July 2022; published 28 July 2022)

The gain and loss in photonic lattices provide possibilities for many functional phenomena. In this Letter, we consider photonic topological insulators with different types of gain-loss domain walls, which will break the translational symmetry of the lattices. A method is proposed to construct effective Hamiltonians, which accurately describe states and the corresponding energies at the domain walls for different types of photonic topological insulators and domain walls with arbitrary shapes. We also consider domain-induced higher-order topological states in two-dimensional non-Hermitian Aubry-André-Harper lattices and use our method to explain such phenomena successfully. Our results reveal the physics in photonic topological insulators with gain-loss domain walls, which provides advanced pathways for manipulation of non-Hermitian topological states in photonic systems.

DOI: 10.1103/PhysRevLett.129.053903

Introduction.—A photonic topological insulator (PTI) is a photonic crystal that behaves as an insulator in its interior while its boundaries provide robust transport channels. According to the photonic band theory and the bulk-boundary correspondence, when a PTI is coupled to another system that resides in a different topological phase, the adjacent part, called the domain wall, will provide topological channels [1–3], which support topological states [4–10], or even higher-order topological states [11–19]. The existence of such channels is protected by the bulk properties of PTIs, leading to their robustness against disorders. The above phenomena have been confirmed in various types of PTIs, including those characterized by Chern numbers [20,21], spin Chern numbers [22], valley Chern numbers [23,24], or bulk polarization [25]. PTIs' characteristic properties have been widely used in low-loss waveguides, robust delay lines, and topological light sources [26–30]. Nevertheless, these configurations usually have difficulties with flexible control of topological states.

As non-Hermitian effects can be useful in practical applications, the frontiers of topological materials and devices research extend into non-Hermitian systems [31–36]. Unlike electronic systems, optical electromagnetic waves transmitting in materials can exhibit gain or loss responses, providing a functional platform for quantitively controlling non-Hermitian effects. It has been reported that adding certain gain and loss in unit cells can lead to a topological phase transition in photonic lattices [37–40]. These systems still have translational symmetries, which allow us to study their properties by topological band theory. Just like the Hermitian case, topological states will appear at the domain wall when combining two topological distinct systems, for example, a non-Hermitian PTI and its Hermitian, topological trivial counterpart. Recently, it has been shown that a single gain-loss domain wall in a gauge field system can support topological edge states, while two domains that make up the domain wall are topological equivalent [41]. However, it usually requires solving non-Hermitian matrices with large dimensions to study such phenomena due to the lack of translational symmetry. So far, there is no general and simple method to analyze PTIs with gain-loss domain walls, especially in systems with multidomain walls and in a broader range of topological systems.

In this Letter, we consider a PTI with several gain-loss domains. We show that localized states will appear at

domain walls when we increase the difference of gain and loss between adjacent domains. Such a phenomenon can be understood by the coupling of topological states of different domains. Based on this, we construct effective Hamiltonians and develop a fitting method to determine it, which gives accurate descriptions of these states and the corresponding energies. The above method also reveals domain-induced higher-order topological states in certain kinds of PTIs. As a concrete verification, we use a cross-shaped domain wall to generate corner states in a two-dimensional(2D) Aubry-André-Harper (AAH) lattice [20,42,43] (as a representative of Chern insulators) and use effective Hamiltonians to explain its properties.

Model.—To illustrate our basic ideas, consider a block of Hermitian PTI. One can introduce a gain or loss effect in different regions such that the PTI is partitioned into several domains by gain-loss domain walls. From another perspective, the Hamiltonian of such a non-Hermitian PTI can be written as $H = \sum_i H_{\mathrm{G},i} + \sum_j H_{\mathrm{L},j} + \sum H'_{ij}$, where the subscripts G and L represent "gain" and "loss," i and j label different domains, and the interaction between two domains is denoted by H'. Now suppose that in each domain, gain (or loss) just provides a constant on-site imaginary potential $+i\gamma_i(-i\gamma_j)$. This will just result in a pure imaginary shift in the spectra of $H_{\mathrm{G},i}(H_{\mathrm{L},j})$. Therefore, $H_{\mathrm{G},i}(H_{\mathrm{L},j})$ also supports topological edge states individually due to the topological nature of the PTI, even with non-Hermiticity. We will next show that the behaviors at domain walls can be succinctly described by the coupling of these non-Hermitian topological states. We choose the AAH model as a concrete example of a PTI characterized by the Chern number to verify the effective Hamiltonian. Our method can also be used for other models. Detailed numerical analyses of the Su-Schrieffer-Heeger model [25], the valley-typed [24] and the C_{6v}-typed [22] photonic crystals in both topological and trivial cases are provided in the Supplemental Material, Sec. I [44].

Domain-induced edge states.—Consider a 1D AAH chain with a tight-binding Hamiltonian

$$H_{\mathrm{1D}} = \sum_{n=1}^{N}(\Omega_n + i\gamma_n)c_n^\dagger c_n + \sum_{n=1}^{N-1}(tc_n^\dagger c_{n+1} + \mathrm{H.c.}), \qquad (1)$$

where $c_n^\dagger(c_n)$ is the creation(annihilation) operator on the nth site. $\Omega_n = V\cos[2\pi\beta(n-q)+\phi]$ is the on-site potential and an offset q is introduced in the cosine modulation [18]. γ_n represents the on-site gain or loss term. In the Hermitian case($\gamma_n = 0$), the above Hamiltonian reflects properties of a 2D Chern insulator with a synthetic ϕ dimension. To construct the domain wall, we set $\gamma_n = \gamma_1$ for $n \le N_1$ and $\gamma_n = -\gamma_2$ for the remaining part [see Fig. 1(a)]. Without loss of generality, we choose $\gamma_1 = \gamma_2 = \gamma > 0$ since we can always do this by setting the zero point of the imaginary potential as $(\gamma_1+\gamma_2)/2$. We will normalize all quantities with t unless specified otherwise. For this

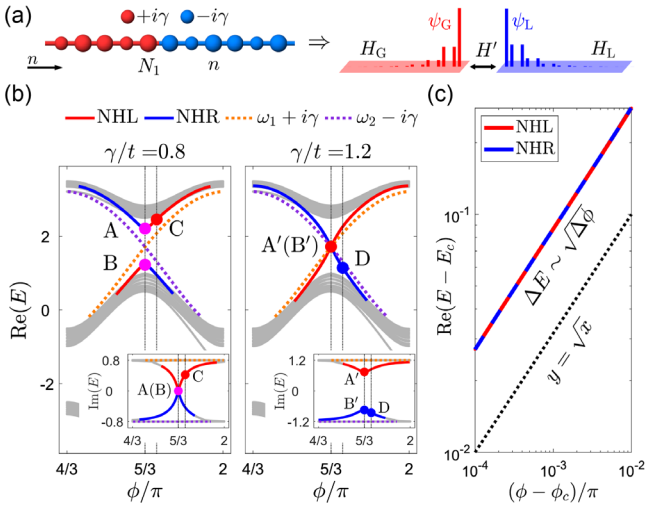

FIG. 1. (a) Schematic diagrams of the 1D-AAH model with non-Hermitian domain walls. (b) Part of the ϕ spectrum of non-Hermitian 1D-AAH chain described by Eq. (1). Domain-induced edge states are colored in red (blue), whose wave functions concentrate in the left(right) region of the domain wall. Inner plot: corresponding imaginary parts of the spectrum. (c) At $\gamma = \gamma_c$, the dispersion relations of two domain-induced bands have the square root form.

choice, Eq. (1) can be written as $H_{\mathrm{1D}} = H_{\mathrm{G}} + H_{\mathrm{L}} + H'$, $H' = tc_{N_1}^\dagger c_{N_1+1} + \mathrm{H.c.}$, according to our basic model. Figure 1(b) shows parts of the real and imaginary ϕ spectrums with parameters $N = 48$, $N_1 = 23$, $V = 3$, $\beta = 1/3$, $q = 2$, and $\gamma/t = 0.8$, 1.2, respectively. As γ/t increases, we find in the ϕ spectrum that certain bands gradually appear in the band gap around $\phi_c = 5\pi/3$. There exists a critical γ_c ($\gamma_c/t \approx 0.94$). When $\gamma \ge \gamma_c$ the emerging bands form an intersection in the middle of the band gap at ϕ_c. Six representative points are selected and the corresponding normalized field distributions are given in Fig. 2(c), which clearly show that these bands represent the states localized at the domain wall.

To explain such phenomenon, eigenenergies of the right edge mode of H_G and the left edge mode of H_L are shown in Fig. 1(b) in orange and purple dot lines, which satisfy $H_G\psi_G = (\omega_1 + i\gamma)\psi_G$, $H_L\psi_L = (\omega_2 - i\gamma)\psi_L$. One can see that we have $\omega_1 = \omega_2$ at ϕ_c. Also, close to ϕ_c, we find that dispersion relations of the two emerging bands have a square root form when $\gamma = \gamma_c$ [Fig. 1(c)]. The behaviors at the domain wall can be understood by considering the coupling of edge channels of $H_{G,L}$. Define $\psi = (\psi_G, \psi_L)^T$, we give the effective Hamiltonian

$$H_{\mathrm{eff}} = \begin{pmatrix} \varepsilon_1 + i\gamma_{\mathrm{eff}} & \kappa \\ \kappa^* & \varepsilon_2 - i\gamma_{\mathrm{eff}} \end{pmatrix}. \qquad (2)$$

Here, nondiagonal elements of H_{eff} are conjugate pairs because the system is reciprocal. At $\phi = \phi_c$, we should have $\varepsilon_1 = \varepsilon_2$. Notice we also have $\omega_1 = \omega_2 = \omega$ at this

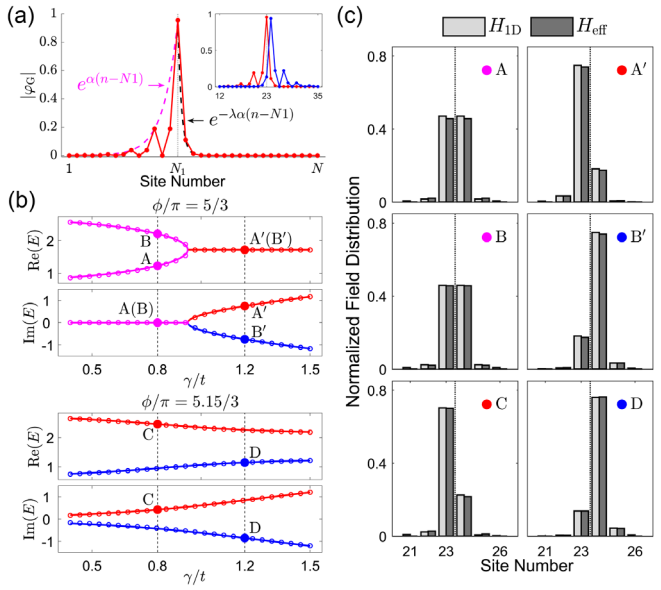

FIG. 2. (a) Schematic plot of constructing φ. (b) Comparison of eigenvalues of domain-induced edge states given by H_{1D} (solid lines) and H_{eff} with $\lambda = 9$ (discrete circles). (c) Comparison of normalized field distributions of six representative domain-induced edge states. Only six sites around the domain wall are shown.

point, a proper choice is to set $\varepsilon_{1,2} = \omega_{1,2}$. As for γ_{eff}, we choose $\gamma_{eff} = \gamma$ since all states of subsystem $H_G(H_L)$ have this gain(loss). The effective Hamiltonian modeling the domain wall is PT symmetric only at $\phi = \phi_c$, and its two basis for the solution space are given by $\psi_\pm \propto e^{-i\omega t}e^{E_\mp t}(c_\pm, 1)^T$. Here $E_\mp = \mp\sqrt{\gamma^2 - \kappa^2}$, $c_\pm = (-i\gamma \pm \sqrt{\kappa^2 - \gamma^2})/\kappa$. Two domain-induced edge states are given by $c_\pm\psi_G + \psi_L$. When $|\gamma| < |\kappa|$, we have $|c_+| = |c_-| = 1$, which results in states A and B. While for $|\gamma| > |\kappa|$, we have $|c_-| > 1$, $|c_+| < 1$, resulting in state A' and B', respectively. Furthermore, notice that a variation in ϕ leads to a 2D topological charge pumping in the synthetic dimension [43]. For ψ_G, such pumping accumulates charges at the boundary, while for ψ_L the boundary charges tend to disperse into the bulk. From this perspective, the net accumulation of charges at the domain wall is zero for section $|\gamma| < |\kappa|$ and nonzero for section $|\gamma| > |\kappa|$ when varying ϕ, which yields $\gamma_c = |\kappa|$ is actually a phase transition point. In the case $\phi \neq \phi_c$, $\omega_1 \neq \omega_2$, ψ is always made up of unequal $\psi_{G,L}$, resulting in states C and D.

The value of coupling coefficient κ is determined through a fitting method. Notice that $\psi_{G,L}$ are exponentially localized at each side of the domain wall with $\psi_G = A_G(n)e^{\alpha_G(n-N_1)}$ and $\psi_L = A_L(n)e^{-\alpha_L(n-N_1-1)}$, $n = 1, 2, \ldots, N$, $A_G(n > N_1) = B_L(n \leq N_1) = 0$. $\alpha_{G,L}$ are the penetration depth and can be calculated from the envelope of $\psi_{G,L}$. To get a fine-tuning of κ, we introduce

$$\varphi_G(n) = \psi_G + B_G(n)e^{-\lambda\alpha_G(n-N_1)},$$
$$\varphi_L(n) = \psi_L + B_L(n)e^{\lambda\alpha_L(n-N_1-1)}, \quad (3)$$

with $B_G(n \leq N_1) = B_L(n > N_1) = 0$, $B_G(n > N_1) = \psi_G(N_1), B_L(n \leq N_1) = \psi_L(N_1 + 1)$. λ is a fitting parameter describing the ratio between the exponential decay of the wave function on the two sides of the domain wall [see Fig. 2(a)]. Then fitting of κ is now turned into the fitting of λ, and their relation is given by

$$\kappa(\lambda) = \langle\varphi_G|H_{1D}|_{\gamma=0}|\varphi_L\rangle. \quad (4)$$

Here, using Hermitian Hamiltonians implies that the coupling strength is not affected by the non-Hermitian term, as has been shown in previous works [45–47]. We quantify the differences between the eigenvalues given by H_{1D} and H_{eff} with different λs near the phase transition point and we find $\lambda \approx 9$ gives the best match (see the Supplemental Material Sec. II [44]). Figure 2(b) compares the $E - \gamma/t$ relation of the two domain-induced edge states at $\phi = 5\pi/3$ and $\phi = 5.15\pi/3$ and Fig. 2(c) compares six representative eigenstates. Our effective Hamiltonian provides a correct physical picture. Though we only show the fitting results in limited parameter regimes, our method can also be applied to broader ranges of ϕ's and γ's.

Domain-induced corner states.—This kind of method can also be applied to analyze domain walls in higher-order topological insulators. Consider a 2D AAH lattice with Hamiltonian

$$H_{2D} = \sum_{n=1}^{N_x}\sum_{m=1}^{N_y}(\Omega_{n,m} + i\gamma_{n,m})c^\dagger_{n,m}c_{n,m} + \sum_{n=1}^{N_x-1}\sum_{m=1}^{N_y-1}(t_x c^\dagger_{n,m}n_{n+1,m} + t_y c^\dagger_{n,m}c_{n,m+1} + \text{H.c.}), \quad (5)$$

where $c^\dagger_{n,m}(c_{n,m})$ is the creation(annihilation) operator on the (n, m) site. $\Omega_{n,m} = V_x\cos[2\pi\beta_x(n - q_x) + \phi_x] + V_y\cos[2\pi\beta_y(m - q_y) + \phi_y]$ provides the on-site potential. $\gamma_{n,m}$ represents the on-site gain/loss term. We set $\gamma_{n,m} = \gamma$ for $n \leq N_1$, $m \leq N_2$, and $n > N_1$, $m > N_2$(region II, IV) while $\gamma_{n,m} = -\gamma$ for the remaining parts(region I, III) such that the domain walls form a cross structure located at (N_2, N_1) [Fig. 3(a)]. The parameters are chosen as $N_x = N_y = 30$, $N_2 = N_1 = 16$, $V_x = V_y = 3$, $\beta_x = \beta_y = 1/3$, and $t_x = t_y = t = 1$. In the Hermitian case ($\gamma_{n,m} = 0$), Eq. (5) can be written as $H_{2D} = I_y \otimes H_{1D,x} + H_{1D,y} \otimes I_x$, thus reflecting properties in a four-dimensional (4D) parameter space (x, y, ϕ_x, ϕ_y). Eigenstates of H_{2D} are the direct product of two eigenstates of H_{1D}, $|\psi_{2D}\rangle = |\psi_{1D,x}\rangle \otimes |\psi_{1D,y}\rangle$. This idea provides us with the principle to determine a subspace, in which H_{2D} can support topological corner states, in the whole 4D phase

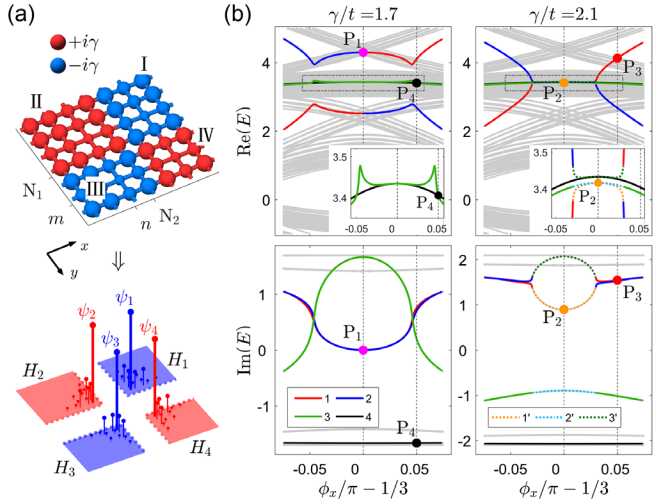

FIG. 3. (a) Layout of a 2D-AAH model with a cross-shaped domain wall. (b) Real and imaginary ϕ spectrum of Eq. (5) on the plane $\phi_x = \phi_y$ in the neighborhood of $\phi_x = \pi/3$. Only domain induced corner states are colored. Inner plot: The enlarged drawing of the gray dot-dash box.

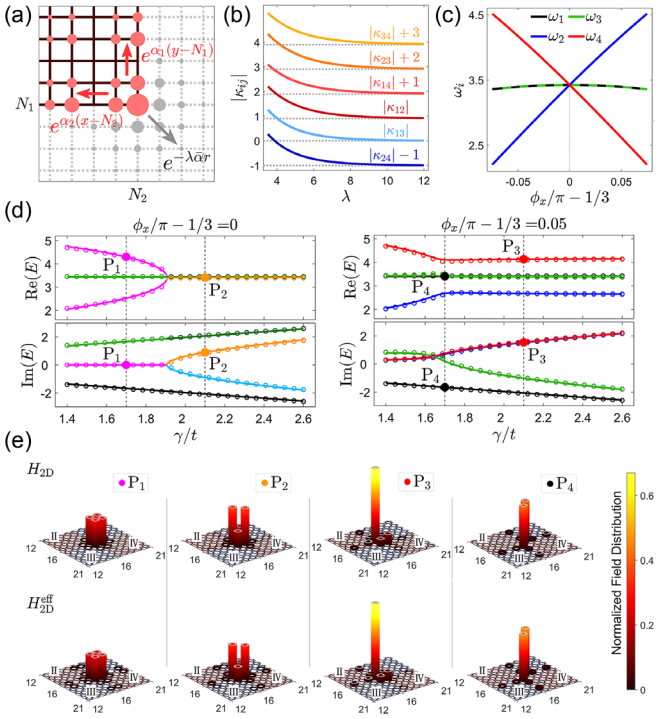

FIG. 4. (a) Schematic plot for constructing assistant states φs in the 2D case. (b) Relations between κ_{ij} and λ. Some quantities have been shifted by a constant for a better distinction. (c) ω's at different ϕ_x's. We always have $\omega_1 = \omega_3$. (d) Comparison of eigenvalues of four domain-induced corner states given by H_{2D} (solid lines) and H_{2D}^{eff} with $\lambda = 9.5$ (discrete circles). (e) Comparison of normalized field distributions of four chosen states around the intersection.

space [18,44,48]. In the non-Hermitian case, by treating the gain or loss term as a perturbation, we can conclude that domain-induced corner states must appear in the neighboring of the related subspace; that is, around $\phi_x = \phi_y = \pi/3$ for the above parameters.

Figure 3(b) shows part of the 2D ϕ spectrums of H_{2D} on the plane $\phi_x = \phi_y$ with $\gamma/t = 1.7$ and 2.1. We only highlight the corner states localized strongly at the middle four sites, even if there are many localized states supported by such domain walls (see the Supplemental Material, Sec. IV [44]). It can be seen that a bridge-shaped intersection gradually forms in the band structure when increasing γ/t. There is always a near flat band (colored black, band 4), whose wave function is supported equally in region I and III. When γ is small, states related to bands 1, 2 concentrate in region II and IV, respectively. For each ϕ there is one state left, we color it green (band 3). When increasing γ, bands 1, 2, 3 approximately overlap in the center, resulting in three new bands $1'$, $2'$, and $3'$. Several typical states are shown in Fig. 4(b) (see Supplemental Material Sec. III for more detailed field distributions at different ϕ_x's [44]).

Just like what we did in the 1D case, H_{2D} can be written as $H_{2D} = \sum_{i=1}^{4} H_i + \sum_{i,j=1}^{4} H'_{ij}$. The effective Hamiltonian H_{eff}^{2D} can be constructed by considering the coupling of four corner channels (ψ_i, $i = 1$–4) that make up the cross-shaped domain walls. ψ_i satisfies $H_i\psi_i = (\omega_i \pm i\gamma)\psi_i$ ("+" for $i = 2$, 4 and "−" for $i = 1$, 3). The coupling coefficient between ψ_i and ψ_j is given by $\kappa_{ij}(\lambda) = \langle\varphi_i|H_{2D}|_{\gamma=0}|\varphi_j\rangle$. φ_i can be constructed from ψ_i by introducing an exponential decay outside the related subsystem, just like the 1D case [see Fig. 4(a)]. Here, we turn a six-dimensional fitting of κ_{ij}s into the fitting of a single parameter λ, since the four subsystems are divided from one bulk. Figure 4(b) shows the value of $|\kappa_{ij}|$ when varying λ. The results allow us to set $|\kappa_{13}| = |\kappa_{24}| = 0$ and $|\kappa_{12}| = |\kappa_{14}| = |\kappa_{23}| = |\kappa_{34}|$ for preliminary theoretical analysis. Since we have $\omega_1 = \omega_3 = \omega(\phi)$ for all ϕs [see Fig. 4(c)], H_{eff}^{2D} always has an eigenstate with probability density $(1/2, 0, 1/2, 0)^T$, whose eigenvalue is $\omega - i\gamma$. This kind of state is related to band 4 observed above. The remaining states can be considered as a trade-off between two effects. Close to $\phi_x = \pi/3$, we also have $\omega_2 \approx \omega_4 \approx \omega$, making H_{eff}^{2D} nearly PT symmetric. When increasing γ, H_{eff}^{2D} becomes PT broken, which leads to bands $1'$–$3'$. Besides, away from $\phi_x = \pi/3$, the difference between ω_2 and ω_4 becomes relevant, promoting asymmetric effects and results in band 1 and 2. When $\phi_x > (<)\pi/3$, we have $\omega_2 > (<)\omega_4$, so the upper and lower relation of band 1 and 2 exchange at the two sides of $\phi_x = \pi/3$. Figures 4(d) and 4(e) compare the $E - \gamma/t$ relationship of the four target states and field distributions of typical domain-induced corner states given by H_{2D} and H_{eff}^{2D} with $\lambda = 9.5$. We achieve precise descriptions by adjusting only one parameter λ.

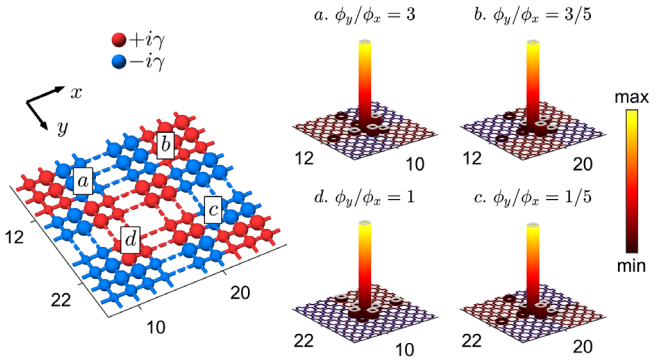

FIG. 5. A multidomain wall configuration and typical density plots at each domain corner.

We finally show that our method is also applicable for behaviors at domain walls with different positions and shapes. Figure 5 shows a configuration, where several domains form 4 domain corners a, b, c, and d. These domain corners support domain-induced localized states in different subspaces of (ϕ_x, ϕ_y). Domain corners a–c are similar to what we have studied here, except for the positions of crossings. A P_3-typed state is found in each case. As for case d, the related behavior should be analyzed by considering the coupling of an L-shaped loss domain and the adjacent square gain domain. Furthermore, by flexibly controlling the shapes and gain or loss of each domain, we can design systems with specific physics. For example, a third order exceptional point composed of domain-induced corner states. Detailed analyses of non-cross-shaped domain walls are shown in the Supplemental Material Sec. V [44].

Conclusion.—We have proposed a universal method to construct effective Hamiltonians. They can give faithful descriptions of the eigenenergies and field distributions of domain induced states, after determining their parameters through our fitting scheme. The method can also be extended to higher dimensional cases and other types of PTIs. We point out that such localized states in PTIs are protected by the topology of the related Hermitian system. We also simulate non-Hermitian AAH arrays for possible experimental realizations of the domain-induced states. The results are shown in the Supplemental Material Sec. VI [44]. The basic principle of our method, that is, behaviors at gain-loss domain walls can be understood via the coupling of subsystems, can be adapted to broader cases, for example, gain-loss domain walls with different positions and shapes in nonreciprocal bulk or trivial photonic crystals, except for possible changes in details of the fitting processes.

This work was supported by the National Key Research and Development Program of China under Grant No. 2018YFB2200403, the National Natural Science Foundation of China under Grants No. 11734001, No. 91950204, No. 92150302, No. 91850117, No. 11654003, Beijing Institute of Technology Research Fund Program for Teli Young Fellows, and the Max Planck-New York City Center for Nonequilibrium Quantum Phenomena. Work done in Hong Kong is supported by RGC Hong Kong through 16303119 and AoE/P-502/20.

*These authors contribute equally to this work.
†Corresponding author.
xiaoyonghu@pku.edu.cn
‡Corresponding author.
cuicuilu@bit.edu.cn
§Corresponding author.
phchan@ust.hk

[1] Z. Wang, Y. Chong, J. D. Joannopoulos, and M. Soljačić, Nature (London) **461**, 772 (2009).
[2] L. Lu, J. D. Joannopoulos, and M. Soljačić, Nat. Photonics **8**, 821 (2014).
[3] T. Ozawa, H. M. Price, A. Amo, N. Goldman, M. Hafezi, L. Lu, M. C. Rechtsman, D. Schuster, J. Simon, O. Zilberberg, and I. Carusotto, Rev. Mod. Phys. **91**, 015006 (2019).
[4] J.-W. Dong, X.-D. Chen, H. Zhu, Y. Wang, and X. Zhang, Nat. Mater. **16**, 298 (2017).
[5] Y. Yang, Y. Yamagami, X. Yu, P. Pitchappa, J. Webber, B. Zhang, M. Fujita, T. Nagatsuma, and R. Singh, Nat. Photonics **14**, 446 (2020).
[6] M. I. Shalaev, W. Walasik, A. Tsukernik, Y. Xu, and N. M. Litchinitser, Nat. Nanotechnol. **14**, 31 (2019).
[7] Y. Ao, X. Hu, C. Li, Y. You, and Q. Gong, Phys. Rev. Mater. **2**, 105201 (2018).
[8] R.-C. Shiu, H.-C. Chan, H.-X. Wang, and G.-Y. Guo, Phys. Rev. Mater. **4**, 065202 (2020).
[9] S. Raghu and F. D. M. Haldane, Phys. Rev. A **78**, 033834 (2008).
[10] S. Barik, A. Karasahin, C. Flower, T. Cai, H. Miyake, W. DeGottardi, M. Hafezi, and E. Waks, Science **359**, 666 (2018).
[11] M. Kim and J. Rho, Nanophotonics **9**, 3227 (2020).
[12] W. A. Benalcazar, B. A. Bernevig, and T. L. Hughes, Science **357**, 61 (2017).
[13] Y. Ota, F. Liu, R. Katsumi, K. Watanabe, K. Wakabayashi, Y. Arakawa, and S. Iwamoto, Optica **6**, 786 (2019).
[14] B. Xie, G. Su, H.-F. Wang, F. Liu, L. Hu, S.-Y. Yu, P. Zhan, M.-H. Lu, Z. Wang, and Y.-F. Chen, Nat. Commun. **11**, 3768 (2020).
[15] J. Noh, W. A. Benalcazar, S. Huang, M. J. Collins, K. P. Chen, T. L. Hughes, and M. C. Rechtsman, Nat. Photonics **12**, 408 (2018).
[16] Y. Liu, S. Leung, F.-F. Li, Z.-K. Lin, X. Tao, Y. Poo, and J.-H. Jiang, Nature (London) **589**, 381 (2021).
[17] W. A. Benalcazar, T. Li, and T. L. Hughes, Phys. Rev. B **99**, 245151 (2019).
[18] Z.-G. Chen, W. Zhu, Y. Tan, L. Wang, and G. Ma, Phys. Rev. X **11**, 011016 (2021).
[19] L. He, Z. Addison, E. J. Mele, and B. Zhen, Nat. Commun. **11**, 3119 (2020).
[20] Y. E. Kraus, Y. Lahini, Z. Ringel, M. Verbin, and O. Zilberberg, Phys. Rev. Lett. **109**, 106402 (2012).
[21] S. A. Skirlo, L. Lu, and M. Soljačić, Phys. Rev. Lett. **113**, 113904 (2014).

[22] L.-H. Wu and X. Hu, Phys. Rev. Lett. **114**, 223901 (2015).
[23] H. Pan, Z. Li, C.-C. Liu, G. Zhu, Z. Qiao, and Y. Yao, Phys. Rev. Lett. **112**, 106802 (2014).
[24] J.-W. Dong, X.-D. Chen, H. Zhu, Y. Wang, and X. Zhang, Nat. Mater. **16**, 298 (2017).
[25] W. A. Benalcazar, B. A. Bernevig, and T. L. Hughes, Phys. Rev. B **96**, 245115 (2017).
[26] Z. Wang, Y. D. Chong, J. D. Joannopoulos, and M. Soljačić, Phys. Rev. Lett. **100**, 013905 (2008).
[27] M. J. Ablowitz and Y.-P. Ma, Opt. Lett. **40**, 4635 (2015).
[28] M. Hafezi, E. A. Demler, M. D. Lukin, and J. M. Taylor, Nat. Phys. **7**, 907 (2011).
[29] H. Zhao, P. Miao, M. H. Teimourpour, S. Malzard, R. El-Ganainy, H. Schomerus, and L. Feng, Nat. Commun. **9**, 981 (2018).
[30] B. Bahari, A. Ndao, F. Vallini, A. El Amili, Y. Fainman, and B. Kanté, Science **358**, 636 (2017).
[31] J. M. Zeuner, M. C. Rechtsman, Y. Plotnik, Y. Lumer, S. Nolte, M. S. Rudner, M. Segev, and A. Szameit, Phys. Rev. Lett. **115**, 040402 (2015).
[32] S. Weimann, M. Kremer, Y. Plotnik, Y. Lumer, S. Nolte, K. G. Makris, M. Segev, M. C. Rechtsman, and A. Szameit, Nat. Mater. **16**, 433 (2017).
[33] S. Yao, F. Song, and Z. Wang, Phys. Rev. Lett. **121**, 136802 (2018).
[34] S. Longhi, Phys. Rev. Lett. **122**, 237601 (2019).
[35] C. Yuce and H. Ramezani, Phys. Rev. A **100**, 032102 (2019).
[36] M. Pan, H. Zhao, P. Miao, S. Longhi, and L. Feng, Nat. Commun. **9**, 1308 (2018).
[37] H. Xue, Q. Wang, B. Zhang, and Y. D. Chong, Phys. Rev. Lett. **124**, 236403 (2020).
[38] A. Guo, G. J. Salamo, D. Duchesne, R. Morandotti, M. Volatier-Ravat, V. Aimez, G. A. Siviloglou, and D. N. Christodoulides, Phys. Rev. Lett. **103**, 093902 (2009).
[39] A. A. Sukhorukov, S. V. Dmitriev, S. V. Suchkov, and Y. S. Kivshar, Opt. Lett. **37**, 2148 (2012).
[40] Y. Ao, X. Hu, Y. You, C. Lu, Y. Fu, X. Wang, and Q. Gong, Phys. Rev. Lett. **125**, 013902 (2020).
[41] H. Zhao, X. Qiao, T. Wu, B. Midya, S. Longhi, and L. Feng, Science **365**, 1163 (2019).
[42] L.-J. Lang, X. Cai, and S. Chen, Phys. Rev. Lett. **108**, 220401 (2012).
[43] Y. E. Kraus and O. Zilberberg, Phys. Rev. Lett. **109**, 116404 (2012).
[44] See Supplemental Material at http://link.aps.org/supplemental/10.1103/PhysRevLett.129.053903 for effective Hamiltonians in other systems, the whole band structure of non-Hermitian AAH model, analysis for domain walls with different shapes and positions, and simulation results of non-Hermitian AAH arrays.
[45] Q. Liu, S. Li, B. Wang, S. Ke, C. Qin, K. Wang, W. Liu, D. Gao, P. Berini, and P. Lu, Phys. Rev. Lett. **124**, 153903 (2020).
[46] B. Peng, S. K. Özdemir, S. Rotter, H. Yilmaz, M. Liertzer, F. Monifi, C. M. Bender, F. Nori, and L. Yang, Science **346**, 328 (2014).
[47] K.-H. Kim, M.-S. Hwang, H.-R. Kim, J.-H. Choi, Y.-S. No, and H.-G. Park, Nat. Commun. **7**, 13893 (2016).
[48] Y. E. Kraus, Z. Ringel, and O. Zilberberg, Phys. Rev. Lett. **111**, 226401 (2013).